VETOR

Dynamic Cycle Simulation in Offshore Mooring Fibers: Modified Mathematical Models and Dependence on Invariants of Continuum Mechanics☆

Simulação de Ciclo Dinâmico em Fibras de Amarração Offshore: Modelos Matemáticos Modificados e Dependência de Invariantes da Mecânica do Contínuo

Daniel Magalhães da Cruz[1†], Ivan Napoleão Bastos[2], Ana Lúcia Nazareth da Silva[3], Jakson Manfredini Vassoler[1], Felipe Tempel Stumpf[1], Aleones José da Cruz Júnior[4], Taline Carvalho Martins[5], Fernanda Mazuco Clain[6], Carlos Eduardo Marcos Guilherme[6]

[1]*Graduate Program in Mechanical Engineering (PROMEC), Federal University of Rio Grande do Sul (UFRGS), Porto Alegre, Rio Grande do Sul, Brazil*
[2]*Polytechnic Institute (IPRJ), Rio de Janeiro State University (UERJ), Nova Friburgo, Rio de Janeiro, Brazil*
[3]*Institute of Macromolecule Professor Eloísa Mano (IMA) & Environmental Engineering Program (PEA), Federal University of Rio de Janeiro (UFRJ), Rio de Janeiro, Rio de Janeiro, Brazil*
[4]*Federal Institute of Education, Science and Technology Goiano (IFGoiano), Trindade, Goiás, Brazil*
[5]*Federal Institute of Education, Science and Technology Goiano (IFGoiano), Rio Verde, Goiás, Brazil*
[6]*Policab Stress Analysis Laboratory, Federal University of Rio Grande (FURG), Rio Grande, Rio Grande do Sul, Brazil*
[†]**Corresponding author:** daniel.cruz@ufrgs.br

Abstract

This paper presents a study on the stress-strain simulation of offshore mooring fibers using the Modified Yeoh model. It incorporates the mathematical descriptions (linear, quadratic, cubic, and exponential), also examining the dependence on the strain invariants (I_1 and I_2), thus aiming to improve the accuracy of the numerical description of the constitutive behavior of the fibers. The research methodology includes computational simulations validated by experimental data, focusing on the mathematical construction based on the Modified Yeoh model for representing the constitutive behavior in mechanical hysteresis (loading-unloading), addressing two fibers: high modulus polyethylene (HMPE) and polyester (PET). The simulation results demonstrate the models' ability to describe the stress-strain behavior, but it is clear that a description solely through I_2 is not sufficient for the convergence of the simulation with the experimental data. For the mathematical models, the linear term dependent on I_1 (principal strains) is the most important for the good fitting of experimental data. The smallest error concerning the simulations is obtained for a model with a complete mathematical description and dependence on both invariants, presenting an average error of 0.52% for HMPE and 1.77% for PET. This work provides a framework for simulating and understanding the mechanical responses of mooring fibers in mechanical hysteresis, highlighting the relevance of the mathematical model and invariant dependence coupled with numerical simulation.

☆This article is an extended version of the work presented at the Joint XXVII ENMC National Meeting on Computational Modeling, XV ECTM Meeting on Science and Technology of Materials,held in Ilhéus–Brazil,from October 1st to 4th, 2024.

Keywords

Synthetic multifilaments • Mechanical hysteresis • Fatigue cycles • Strain energy function • Hyperelastic models

Resumo

Este artigo apresenta um estudo sobre a simulação de tensão-deformação de fibras de ancoragem offshore utilizando o modelo de Yeoh Modificado. Ele incorpora descrições matemáticas (linear, quadrática, cúbica e exponencial), além de examinar a dependência dos invariantes de deformação (I_1 e I_2), visando melhorar a precisão da descrição numérica do comportamento constitutivo das fibras. A metodologia de pesquisa inclui simulações computacionais validadas por dados experimentais, com foco na construção matemática baseada no modelo de Yeoh Modificado para representar o comportamento constitutivo na histerese mecânica (carregamento-descarregamento), abordando duas fibras: polietileno de alto módulo (HMPE) e poliéster (PET). Os resultados das simulações demonstram a capacidade dos modelos de descrever o comportamento tensão-deformação, mas fica claro que uma descrição apenas através de I_2 não é suficiente para a convergência da simulação com os dados experimentais. Para os modelos matemáticos, o termo linear dependente de I_1 (deformações principais) é o mais importante para o bom ajuste aos dados experimentais. O menor erro em relação às simulações é obtido para um modelo com uma descrição matemática completa e dependência de ambos os invariantes, apresentando um erro médio de $0,52\%$ para o HMPE e $1,77\%$ para o PET. Este trabalho fornece uma estrutura para simular e compreender as respostas mecânicas das fibras de ancoragem em histerese mecânica, destacando a relevância do modelo matemático e da dependência dos invariantes acoplados à simulação numérica.

Palavras-chave

Multifilamentos sintéticos • Histerese mecânica • Ciclos de fadiga • Função energia de deformação • Modelos hiperelásticos

1 Introduction

In recent decades, advancements in materials engineering have driven growth in academic research, industrial production, and technological applications, particularly in polymers and polymeric fibers [1]. These synthetic fibers often exhibit superior properties and are more cost-effective compared to natural polymers [2], proving essential in various applications, including offshore mooring systems. Specifically, synthetic fibers have replaced steel cables in conventional offshore applications due to their superior mechanical performance in marine conditions, lighter weight, better commissioning operations, lower cost, and resistance to the marine environment [3, 4]. Offshore mooring systems have evolved to provide greater stiffness and limit the movement of floating units, making the study of the mechanical performance of these fibers fundamental [5, 6, 7, 8]. Among the prominent polymeric fibers are polyester, polyamide, and high-modulus polyethylene (HMPE), with polyester being widely used due to its excellent mechanical properties, easy production, relatively low cost, recyclability, and lightness [9, 10]. Polyester is main fiber for Floating Production Storage and Offloading (FPSO), Float Point Unit (FPU), and Mobile Offshore Drilling Units (MODU) mooring systems. While HMPE is one of the highest tenacity fibers, featuring high strength, low breaking elongation (which would enable offshore installations in deeper waters), and buoyancy in water [9, 11, 12]. Regarding HMPE, the literature reports continuous improvements in creep resistance, with the development of Low Creep HMPE fibers [13, 14, 15, 16].

The mechanical characterization of polymeric materials, especially multifilaments, is influenced by various variables. Due to the non-linear nature of these materials, predicting their behavior represents a complex challenge [17]. Therefore, many studies rely on experimental data for analysis, which often come from laboratory mechanical testing, creating experimental-analytical and/or experimental-numerical linkages [18, 19, 20, 21, 22, 23, 24, 25]. Understanding the mechanics of materials is crucial to predicting structural performance in various applications, ensuring the safety and durability of structures. Numerical simulation is a powerful tool to explore the intrinsic behavior of these materials under various loads. Several studies use this computational approach to examine mechanical performance in challenging scenarios for real experiments [26, 27, 28, 29]. Numerical simulation provides valuable insights, revealing complex details about stresses, strains, and other internal variables not easily observable through experimentation.

The recent efforts of the authors have focused on hyperelastic models for simulation modeling and optimization of the behavior of different fibers, including distinct load conditions, methodologies for constructive levels, and energy-strain functions. Stumpf *et al.* [30] address the simulation for four different fibers under cyclic load using the Stumpf-Marczak energy model that meets the Baker-Ericksen inequalities. da Cruz *et al.* [31] address the numerical simulation of stress-strain behavior for hybrid lines in series of polyester and HMPE. Stumpf *et al.* [32] complemented this study for five multimaterial line configurations, proving it is possible to simulate the constitutive behavior of all

configurations with a single set of parameters. da Cruz *et al.* [33] tested different energy-deformation functions for polyester, establishing that the lowest error is found for the Modified Yeoh model. da Cruz *et al.* [34] also presents numerical simulation of stress-strain for different constructive levels: multifilaments and mooring sub-ropes. da Cruz *et al.* [35] presents significant results of stress-strain simulation capacity for polyester and HMPE fibers for rupture, creep, and cyclic load. In da Cruz *et al.* [36], cycle-by-cycle numerical simulations are related to changes in stiffness throughout loading and unloading cycles, providing mechanical significance to some model constants that are phenomenological.

This work aims to analyze the constitutive behavior of HMPE and polyester fibers (multifilament level) for offshore use through numerical simulation, using the modified Yeoh hyperelastic model. The objective is to focus on the stress-strain response and your numeric simulation for a stabilized cycle of mechanical hysteresis (loading and unloading), evaluating the mathematical terms to be incremented in the Modified Yeoh model and their dependencies on the invariants of continuum mechanics. Thus, the strain energy model is evaluated concerning the mathematical construction of the appearing terms (linear, quadratic, cubic, and exponential) and the dependency on the invariants (I_1 and I_2).

In this context, the specific gaps addressed in this study concern the numerical simulation of stabilized mechanical hysteresis in synthetic fibers, particularly under cyclic loading. The main objectives are: (i) to simulate the stress-strain response of HMPE and polyester fibers using the Modified Yeoh hyperelastic model; (ii) to evaluate the influence of additional mathematical terms (linear, quadratic, cubic, and exponential) in the strain energy function; and (iii) to assess the model's sensitivity to the use of different invariants from continuum mechanics (I_1 and I_2). These aspects are systematically investigated and later revisited in the conclusions.

2 Materials and Methods

2.1 Fiber Specification and Experimental Test

The high-modulus polyethylene (HMPE) multifilaments are coded as JX99 and were extracted from virgin spools (Fig. 1, left), presenting has a specific mass of 0.97 g/cm^3 and a linear density of 1600 denier (1777 dtex). The polyester (PET) multifilaments are coded as SFS5202 and also were extracted from virgin spools (Fig. 1, right). The PET used has a specific mass of 1.38 g/cm^3 and a linear density of 2000 denier (2200 dtex).

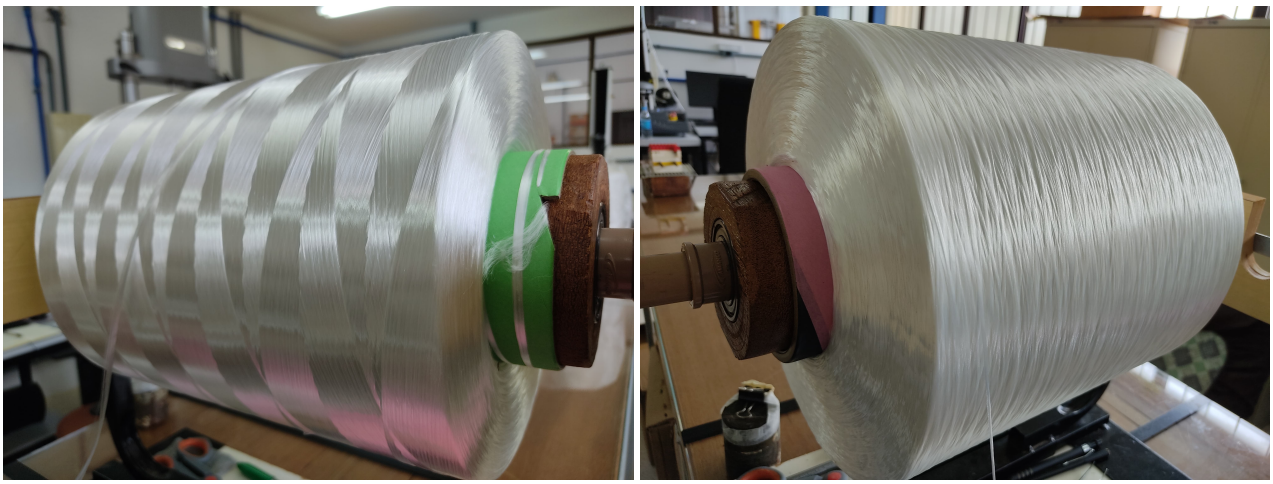

Figure 1: Virgin multifilament spools for specimen extraction: High-modulus polyethylene JX99 with 480 filaments (left); Polyester SFS5202 with 192 filaments (right).

This study aims to run numerical simulations based on experimental fatigue data. The fatigue procedure, in turn, depends on the multifilament's breaking load. Therefore, an experimental characterization of the multifilament was conducted through linear density, Yarn Break Load (YBL), and dynamic tests (loading and unloading).

The linear density test was performed according to ASTM D1577 [37], using an analytical scale (Fig. 2, left), with 9 minutes allocated for the stabilization of each specimen's mass indication, measurement of mass per unit length. The Yarn Break Load (YBL) test was executed in accordance with ISO 2062 [38], using universal testing machine (Fig. 2, center). Specimens with length of 500 mm, an extension rate of 250 mm/min, and a twist condition of 60 turns per meter were tested to determine the breaking force.

The cyclic test was carried out on the Instron E-3000 (Fig. 2, right), with force-control cyclic loading. The maximum load was 45% of the YBL, and the minimum load was 0% of the YBL (zero load). Each specimen underwent 100 cycles at a frequency of 0.1 Hz, resulting in a total test time of 1000 seconds per specimen, which had a standard length of 200 mm.

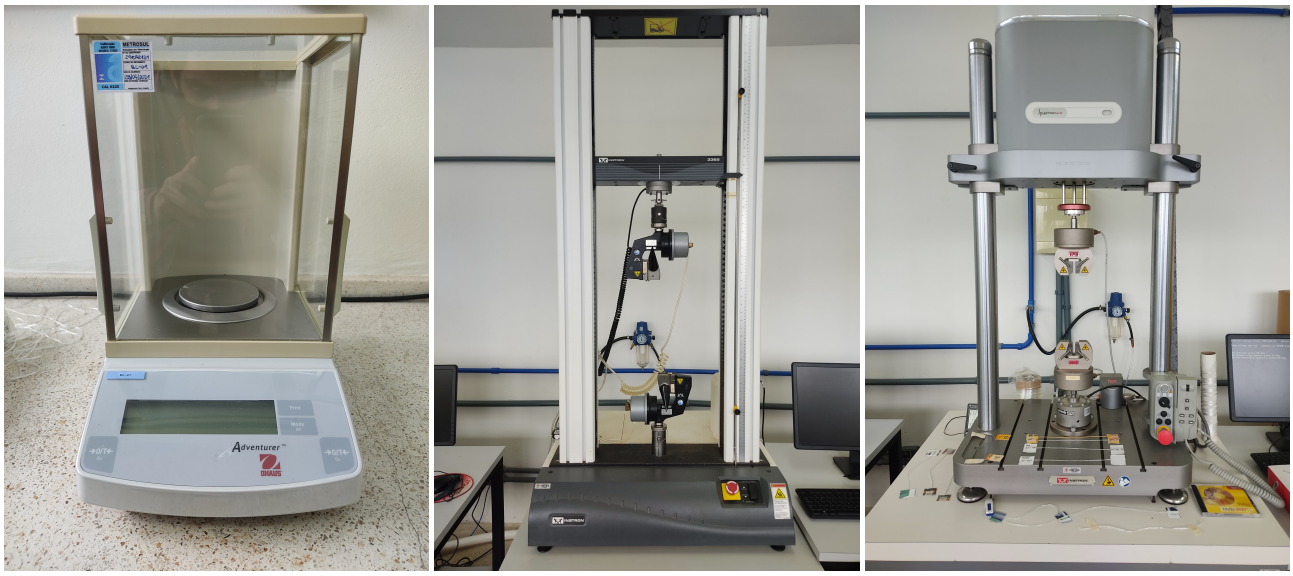

Figure 2: Experimental Test Equipment: Analytical scale (left); Instron 3365 static equipment (center); Instron E-3000 dynamic equipment (right).

In the numerical simulation, the experimental cyclic data are used as a reference to evaluate the simulation and strain energy models. Therefore, understanding the material's mechanical behavior under tensile loading, whether under monotonic or cyclic loads, is essential for the complexity of the model to be employed. In these simulations, the data used will be those obtained from the last fatigue cycle (the hundredth cycle), along with modified hyperelastic models, which will be demonstrated later.

In the tensorial script, data is processed as stress; however, in the multifilament tests, measuring the area is a challenge, making it impossible to rely on stress calculations using the conventional load to area ratio. Therefore, a mathematical approach is employed that combines load, specific mass (ρ), and linear density (ρ_L) to determine the stress (σ), as described in Eq. (1). Dimensional consistency with respect to units is also indicated in Eq. (1).

$$\sigma\,[\text{MPa}] = \frac{F\,[\text{N}] \times \rho\left[\text{g/cm}^3\right]}{\rho_L\,[\text{g/m}]} \tag{1}$$

2.2 Mathematical Description of the Simulation and Optimization

The numerical code was developed based on Simo and Hughes [39], on the theory of elasticity, continuum mechanics, and also on the material properties. The code is developed in MATLAB and has been previously presented in a very similar form in the literature [33, 35].

Considering a body $\Omega \subset \mathbb{R}^3$, subjected to finite deformation $\varphi : \Omega \to \mathbb{R}^3$, the deformation gradient is defined $\boldsymbol{F} = \partial\varphi(\boldsymbol{X})/\partial\boldsymbol{X}$, where $\boldsymbol{X}$ is the material point in the reference (undeformed) configuration, and $J = \det \boldsymbol{F} > 0$ is the Jacobian. The deformation gradient $\boldsymbol{F}$ can be multiplicatively decomposed [40], as shown in Eq. (2). Where $\widehat{\boldsymbol{F}}$ refers to the volumetric part, and $\overline{\boldsymbol{F}}$ refers to the isochoric part, respectively defined in Eq. (3) and Eq. (4). The variable $\boldsymbol{I}$ corresponds to the identity matrix.

$$\boldsymbol{F} = \widehat{\boldsymbol{F}}\overline{\boldsymbol{F}} \tag{2}$$

$$\widehat{\boldsymbol{F}} = J^{1/3}\boldsymbol{I}, \text{ with } \det\widehat{\boldsymbol{F}} = \det\boldsymbol{F} = J \tag{3}$$

$$\overline{\boldsymbol{F}} = J^{-1/3}\boldsymbol{F}, \text{ with } \det\overline{\boldsymbol{F}} = 1 \tag{4}$$

A body under deformation stores energy (strain energy), and this stored energy is written as a strain energy density function, which is a scalar-valued function that relates the strain energy density of a material to the applied deformation, Eq. (5). Where W^{vol} and W^{iso} are the volumetric and volume-preserving (isochoric) portions of the

strain energy function W, respectively. Although the strain energy function is a separate topic (especially due to mathematical modifications), its introduction is important for mathematical and tensorial development. This is because, in the case of incompressible materials, the volumetric part W^{vol} vanishes, leading to work in isochoric terms, Eq. (6).

$$W = W^{\text{vol}} + W^{\text{iso}} \tag{5}$$

$$W = W^{\text{iso}} \tag{6}$$

From Eq. (2), developing the expressions the right Cauchy-Green tensor in the isochoric term ($\overline{\boldsymbol{C}}$) can be written in terms of $\overline{\boldsymbol{C}} = \overline{\boldsymbol{F}}^T\overline{\boldsymbol{F}} = J^{-2/3}\boldsymbol{C}$. With $\det\overline{\boldsymbol{C}} = 1$ and $\boldsymbol{C} = \boldsymbol{F}^T\boldsymbol{F}$, the invariants of continuum mechanics for $\overline{\boldsymbol{C}}$ are determined in Eq. (7), Eq. (8), and Eq. (9).

$$\overline{I_1} = \operatorname{tr}\overline{\boldsymbol{C}} \tag{7}$$

$$\overline{I_2} = \frac{1}{2}\left(\left(\operatorname{tr}\overline{\boldsymbol{C}}\right)^2 - \operatorname{tr}\overline{\boldsymbol{C}}^2\right) \tag{8}$$

$$\overline{I_3} = \det\overline{\boldsymbol{C}} = 1 \tag{9}$$

An internal variable ($\boldsymbol{H}$) is introduced from material properties (τ_i), time step (Δt_n), and Piola-Kirchhoff stress tensor in isochoric terms ($\overline{\boldsymbol{S}}$). Mathematical advancement involves optimization loops for refining energy model constants (C_i) and the tensorial script. The internal variable $\boldsymbol{H}$ updating equation is in Eq. (10), and tensor $\boldsymbol{S}$ is defined in Eq. (11).

$$\boldsymbol{H}_{n+1} = \exp\left(-\frac{\Delta t_n}{\tau_i}\right)\boldsymbol{H}_n + \exp\left(-\frac{\Delta t_n}{2\tau_i}\right)\left(\overline{\boldsymbol{S}}_{n+1} - \overline{\boldsymbol{S}}_n\right) \tag{10}$$

$$\boldsymbol{S} = 2\left(\frac{\partial W}{\partial I_1} + \frac{\partial W}{\partial I_2}\right)\boldsymbol{I} - 2\frac{\partial W}{\partial I_2}\boldsymbol{C} + 2\frac{\partial W}{\partial I_3}I_3\boldsymbol{C}^{-1} \tag{11}$$

Deviatoric functions are calculated for the second Piola-Kirchhoff stress tensor and for the internal variable. Eq. (12) shows the mathematical form of calculating this deviatoric function, where $\mathbf{A}$ denotes a generic second-order tensor (which in development will assume $\mathbf{S}$ or $\mathbf{H}$). It is noteworthy that the operation in brackets in Eq. (12) is an inner product, which can be defined as the trace of the inverse of $\mathbf{A}$ with $\boldsymbol{C}$. The superscript with "$\circ$" indicates the execution of a deviatoric function.

$$\text{DEV}_{n+1}(\mathbf{A}) = (\mathbf{A}) - \frac{1}{3}\cdot[(\mathbf{A}) : \boldsymbol{C}_{n+1}]\,\boldsymbol{C}_{n+1}^{-1} \tag{12}$$

The deviatoric functions associated with the stiffness model of the system and internal variable provide a final stress matrix shown in Eq. (13), which assumes the simplified form of notation on Eq. (14), where "$\circ$" indicates the deviatoric function. Simo and Hughes [39] define that $\gamma_\infty = \gamma - 1$, which corresponds to a stiffness portion of the model. Thus, Eq. (14) is rewritten as Eq. (15).

$$\boldsymbol{S}_{final} = \gamma_\infty\,\text{DEV}_{n+1}(\boldsymbol{S}) + \gamma\,\text{DEV}_{n+1}(\boldsymbol{H}) \tag{13}$$

$$\boldsymbol{S}_{final} = \gamma_\infty\,\boldsymbol{S}^\circ_{n+1} + \gamma\,\boldsymbol{H}^\circ_{n+1} \tag{14}$$

$$\boldsymbol{S}_{final} = (\gamma - 1)\,\boldsymbol{S}^\circ_{n+1} + \gamma\,\boldsymbol{H}^\circ_{n+1} \tag{15}$$

For the final stress expression, as comparing the second Piola-Kirchhoff tensor is impractical, a stress transformation is performed to allow result comparison. Thus, the Kirchhoff (spatial) stress tensor is calculated through the standard transformation, Eq. (16). From the stress already transformed, deformations and stresses are extracted for plotting.

$$\boldsymbol{\sigma}_{n+1} = \boldsymbol{F}_{n+1}\boldsymbol{S}_{final}\boldsymbol{F}^T_{n+1} \tag{16}$$

To evaluate the convergence of the results, it is necessary to quantify the error. Using the experimental stress values as a reference, a point-by-point percentage relative difference calculation is made between the reference stress (σ_{exp}) and numerical stress values (σ_{num}), where the mean of this summation provides an average error value (ϵ), Eq. (17).

$$\epsilon\,[\%] = \frac{1}{n}\sum_{i=1}^{n}\left|\frac{\sigma_{\text{exp}_i} - \sigma_{\text{num}_i}}{\sigma_{\text{exp}_i}} \times 100\right| \tag{17}$$

2.3 Modified Hyperelastic Models

The strain energy function has already been introduced earlier, being an important part of determining the second Piola-Kirchhoff stress tensor presented in Eq. (11). Hyperelastic models are usually the most suitable for highly deformable elastic materials. The hyperelastic material, or Green elastic material, according to Holzapfel [41], postulate the existence of the specific strain energy function W, also called Helmholtz free energy, which can be described for homogeneous and isotropic materials in terms of the invariants $W(I_1, I_2, I_3)$. In this case, considering the material to be incompressible, the third invariant of the tensor is unitary, which is a valid approximation for many polymeric materials and has already been considered in the mathematical and tensorial development, thus $W(I_1, I_2)$.

The proposition of the comparative study of numerical simulation lies precisely in the function W, which corresponds to the adopted strain energy function. Previously, da Cruz *et al.* [33] presented for polyester that the lowest average error was obtained with the Modified Yeoh model [42], Eq. (18). It should be noted that in the construction of this model, there are four types of mathematical terms, namely: linear (L), quadratic (Q), cubic (C), and exponential (E); furthermore, its dependence is only on the first invariant.

$$W = C_1 (I_1 - 3) + C_2 (I_1 - 3)^2 + C_3 (I_1 - 3)^3 + \frac{C_4}{C_5} (1 - \exp(-C_5 (I_1 - 3))) \tag{18}$$

The aim is, therefore, to explore the mathematical construction concomitant with the dependence on the invariants I_1 and I_2. Therefore, three sets of strain energy equations are proposed in relation to the dependence on the invariants, $W(I_1)$, $W(I_2)$, and $W(I_1, I_2)$. Each of these sets has an additive progressive mathematical construction, starting with the linear term, and then adding the quadratic, cubic, and exponential terms for a new numerical simulation.

For the first set of equations, dependent on the first invariant, $W(I_1)$, they are described in Eq. (19) for the linear term and note that this is the Neo-Hook model [43], Eq. (20) for linear and quadratic terms, Eq. (21) for linear, quadratic, and cubic terms, note that this is the Yeoh model [44], and Eq. (22) for the complete mathematical: linear, quadratic, cubic, and exponential terms, note that this is the Modified Yeoh model [42].

$$W = C_1 (I_1 - 3) \tag{19}$$

$$W = C_1 (I_1 - 3) + C_2 (I_1 - 3)^2 \tag{20}$$

$$W = C_1 (I_1 - 3) + C_2 (I_1 - 3)^2 + C_3 (I_1 - 3)^3 \tag{21}$$

$$W = C_1 (I_1 - 3) + C_2 (I_1 - 3)^2 + C_3 (I_1 - 3)^3 + \frac{C_4}{C_5} (1 - \exp(-C_5 (I_1 - 3))) \tag{22}$$

For the second set of equations, dependent on the second invariant, $W(I_2)$, they are described in Eq. (23) for the linear term, Eq. (24) for linear and quadratic terms, Eq. (25) for linear, quadratic, and cubic terms, and Eq. (26) for the complete mathematical: linear, quadratic, cubic, and exponential terms.

$$W = C_1 (I_2 - 3) \tag{23}$$

$$W = C_1 (I_2 - 3) + C_2 (I_2 - 3)^2 \tag{24}$$

$$W = C_1 (I_2 - 3) + C_2 (I_2 - 3)^2 + C_3 (I_2 - 3)^3 \tag{25}$$

$$W = C_1 (I_2 - 3) + C_2 (I_2 - 3)^2 + C_3 (I_2 - 3)^3 + \frac{C_4}{C_5} (1 - \exp(-C_5 (I_2 - 3))) \tag{26}$$

For the third set of equations, dependent on the first and second invariant, $W(I_1, I_2)$, they are described in Eq. (27) for the linear term, note that this is the Mooney-Rivlin model [45, 46], Eq. (28) for linear and quadratic terms, Eq. (29) for linear, quadratic, and cubic terms, and Eq. (30) for the complete mathematical: linear, quadratic, cubic, and exponential terms.

$$W = C_1 (I_1 - 3) + C_2 (I_2 - 3) \tag{27}$$

$$W = C_1 (I_1 - 3) + C_2 (I_2 - 3) + C_3 (I_1 - 3)^2 + C_4 (I_2 - 3)^2 \tag{28}$$

$$W = C_1 (I_1 - 3) + C_2 (I_2 - 3) + C_3 (I_1 - 3)^2 + C_4 (I_2 - 3)^2 + C_5 (I_1 - 3)^3 + C_6 (I_2 - 3)^3 \tag{29}$$

$$W = C_1 (I_1 - 3) + C_2 (I_2 - 3) + C_3 (I_1 - 3)^2 + C_4 (I_2 - 3)^2 + C_5 (I_1 - 3)^3 + C_6 (I_2 - 3)^3 + \frac{C_7}{C_8} (1 - \exp(-C_8 (I_1 - 3))) + \frac{C_9}{C_{10}} (1 - \exp(-C_{10} (I_2 - 3))) \tag{30}$$

3 Results and Discussion

The initial characterization results of the HMPE and polyester multifilament are shown in Table 1. The value of the breaking force corresponds to 100% of the YBL, thus the cyclic loading condition ranging from 0 to 45% YBL, corresponds to 45% of the breaking strength in load (approximately 252 N for high-modulus polyethylene and 82 N for polyester) to be applied in a force-controlled test.

Regarding the values presented in Table 1, the linear density agrees with the typification of 1600 denier for HMPE and 2000 denier for PET, and the rupture strain of 3% for high-modulus polyethylene fibers and 13% for polyester fibers aligns with other studies in the literature [9, 10, 35]. It is worth noting that stress values presented in Table 1 is determined mathematically through Eq. (1) due to the impossibility of measuring the area for calculating the force-to-area ratio (stress by definition).

Table 1: Initial characterization results of HMPE and PET fibers.

	HMPE JX99	PET SFS5202
Linear density [dtex]	1786	2289
Yarn Break Load [N]	560.33	178.45
Breaking stress [MPa]	3043.22	1075.82
Elongation at break [mm]	14.95	66.15
Deformation at break [%]	2.99	13.23
Linear tenacity [N/tex]	3.137	0.780

In Table 1, the linear tenacity values required by standards for mooring ropes are highlighted: at least 2.5 N/tex for HMPE yarns according ISO 18692-3 [47], and 0.78 N/tex for PET yarns according ISO 18692-2 [48].

The experimental results of dynamic cycling are presented in Fig. 3a for high-modulus polyethylene (HMPE) and in Fig. 3b for polyester (PET). It is noteworthy that the cycle used for numerical simulation (100th loading-unloading cycle) is highlighted in each of the plots of the experimental data, in green for HMPE and in magenta for PET. The HMPE shows deformations of up to 1.7–1.8%, while the PET exhibits deformations of 7.9–8.1%. For both fibers, these values represent approximately three-fifths (60%) of the breaking strain (Table 1).

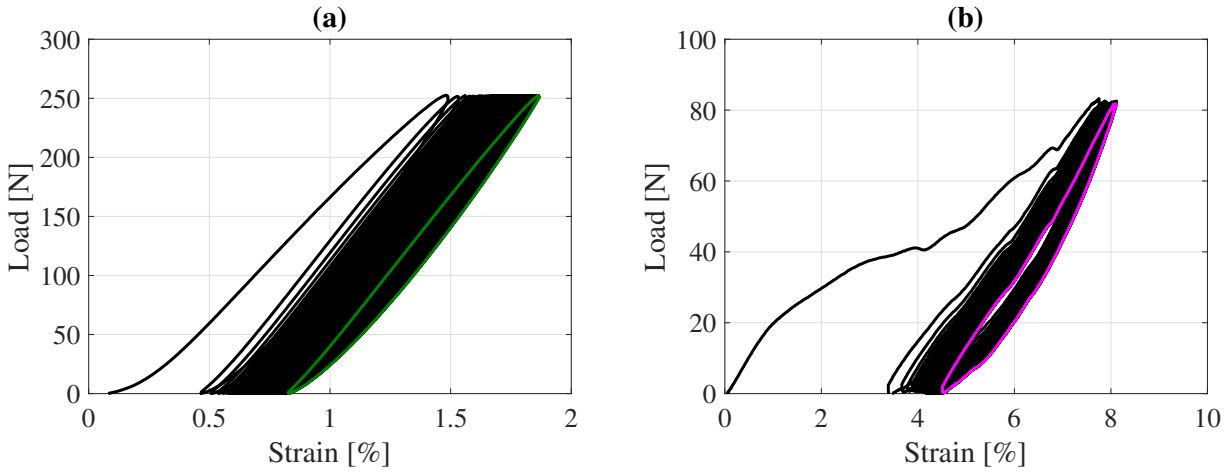

Figure 3: Experimental results of dynamic load cycling tests 0-45% of Yarn Break Load: (a) HMPE; (b) PET.

For the numerical simulation results, these are also plotted along with indications of the experimental data. The simulation results for the first set of equations, dependent solely on the first invariant (I_1), are presented in Fig. 4 for the hundredth cycle for high-modulus polyethylene fibers, and in Fig. 5 for the hundredth cycle for polyester fibers.

From a visual criterion perspective, all numerical simulations with dependence on I_1, regardless of the mathematical formulation, exhibit good agreement in simulating the constitutive behavior of the fiber.

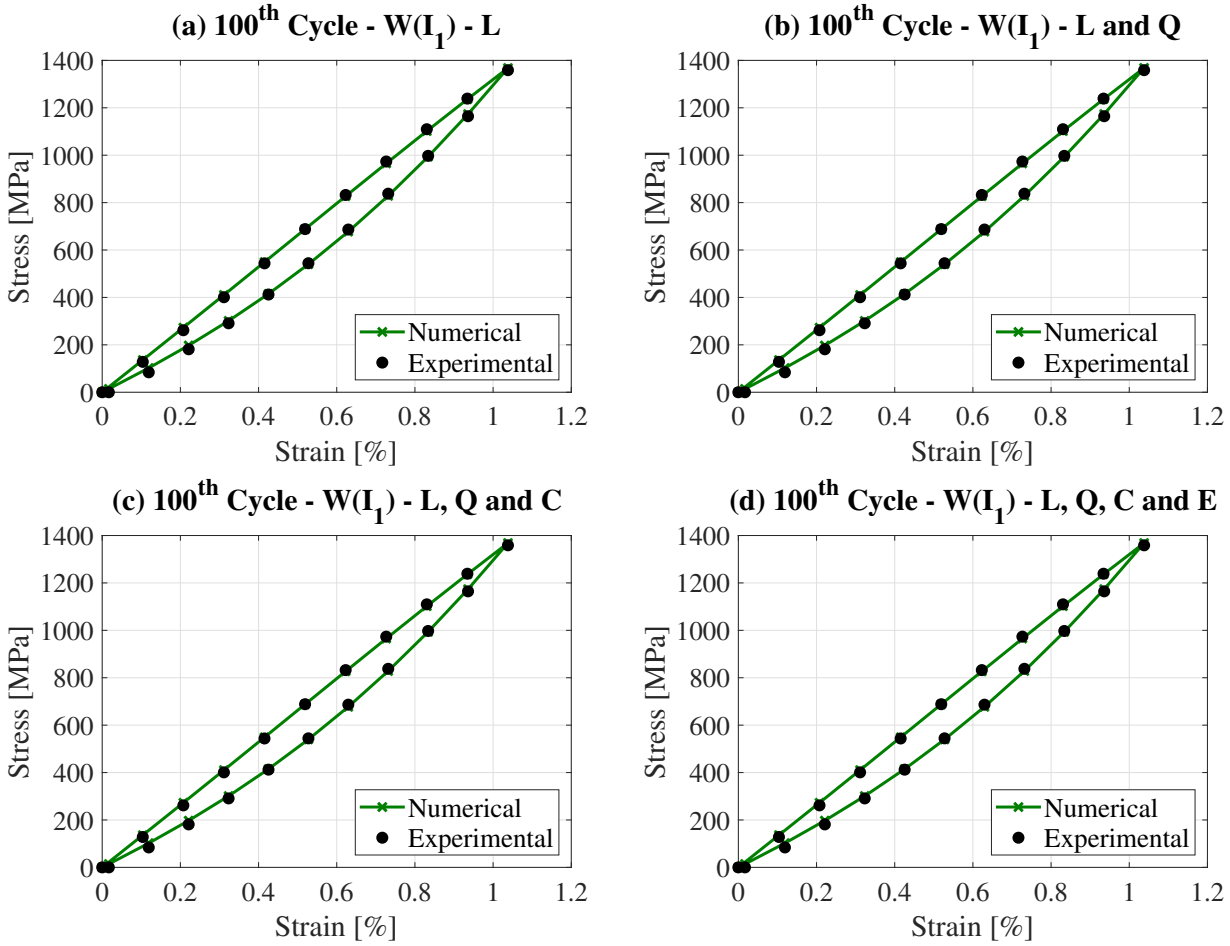

Figure 4: Numerical simulation for dependence on the first invariant, HMPE: (a) Linear; (b) Linear and quadratic; (c) Linear, quadratic and cubic; (d) Linear, quadratic, cubic and exponential.

Similarly, the plots of the numerical simulations along with the experimental data for the second set of equations (Fig. 6 for HMPE, and Fig. 7 for PET) are presented, which depend solely on the second invariant (I_2). Visually, the numerical simulations dependent solely on the second invariant do not show good results for any of the mathematical formulations (and the worse was for the linear term).

This behavior was somewhat expected as the invariants have meanings in continuum mechanics. Similar to the condition of incompressibility being understood as a unitary I_3, the other invariants carry meanings as well. The invariant I_1 captures the sum of principal stretches and is crucial for describing the overall material deformation, as it is closely linked to the elastic components of the material and captures phenomena well in hyperelastic polymeric materials where strains are significant. On the other hand, the invariant I_2 is more directly associated with shear components of deformation, capturing the dot product of principal stretches and reflecting shear deformation components, anisotropic deformation, and directional variations in material properties. In the conducted uniaxial test, deformation primarily occurs longitudinally. The material is not considered anisotropic, and capturing shear deformations is not significant for describing the stress-strain behavior of the fiber.

Continuing with the simulation results, the constitutive numerical plots are presented alongside the experimental data for the third set of equations (Fig. 8 for HMPE, and Fig 9 for PET), which depend on both the first and second invariants (I_1 and I_2). Visually, these numerical simulations converge with the experimental data regardless of the mathematical formulation, requiring a second criterion of average error to assess the best fitting.

As in the graphical construction, many numerical simulations show convergence with respect to the experimental data. The mathematical criterion of average error is used, indicated in Eq. (17), and the results are presented in Table 2 for HMPE, and Table 3 for PET.

For the error values found, similar behaviors can be observed for both fibers. In the equations dependent on the first invariant I_1, only the linear and quadratic terms are significant, as there was no reduction in error with the addition of cubic and exponential terms, although they still show good results with low average error. A similar situation occurs for the second set of equations (dependence only on the second invariant I_2 of continuum mechanics), where

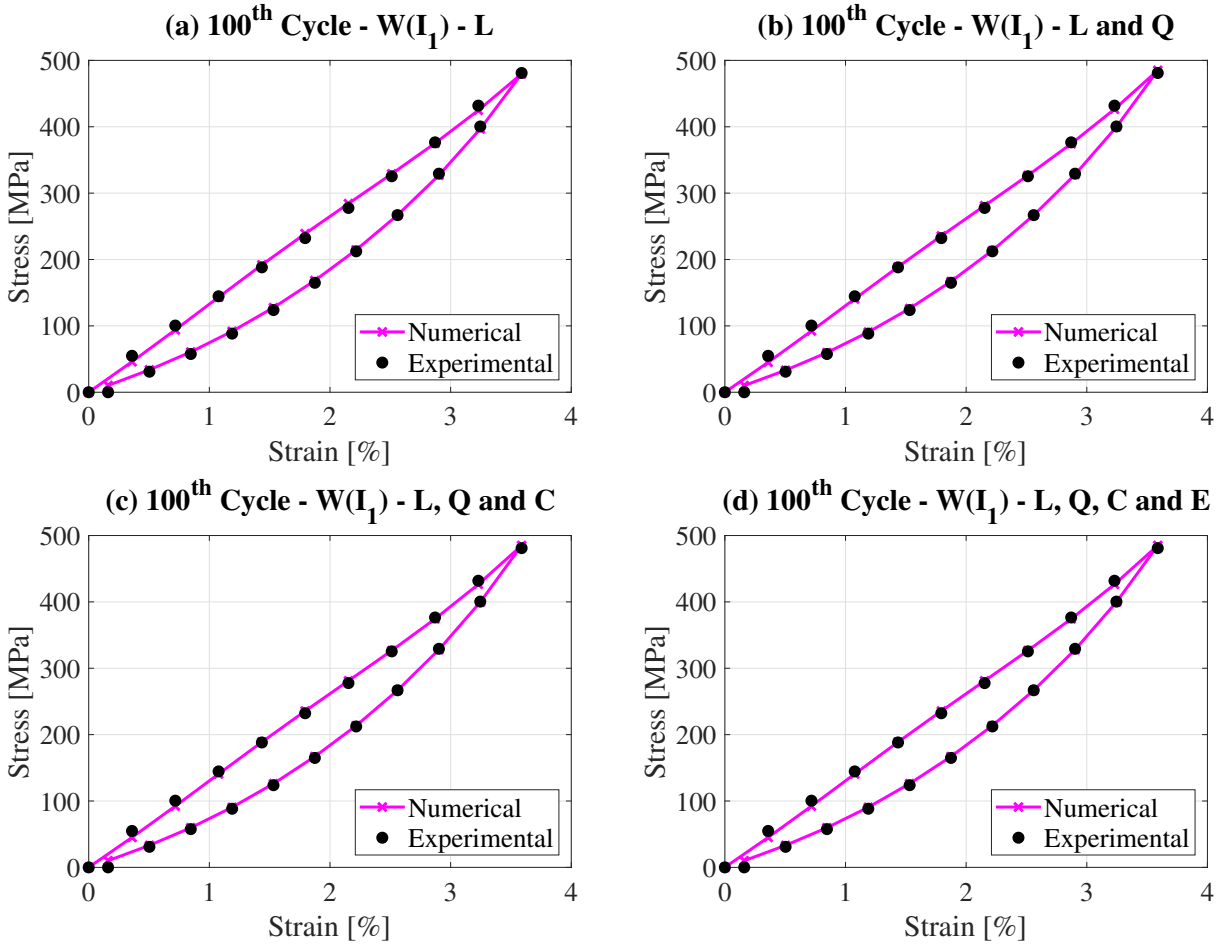

Figure 5: Numerical simulation for dependence on the first invariant, PET: (a) Linear; (b) Linear and quadratic; (c) Linear, quadratic and cubic; (d) Linear, quadratic, cubic and exponential.

Table 2: Average error in percentage for each numerical simulation, HMPE.

	$W(I_1)$	$W(I_2)$	$W(I_1, I_2)$
Linear	2.792	25.399	2.792
Linear and quadratic	2.775	13.271	1.910
Linear, quadratic and cubic	2.775	13.271	0.878
Linear, quadratic, cubic and exponential	2.775	13.271	0.522

only the linear and quadratic terms are significant, and there was no reduction in the average error with the addition of cubic and exponential terms. However, the average errors of the simulations dependent on the second invariant are very high, leading to very poor results for both fibers when dependent on I_2 (as already evident from the graph). Finally, for the dependence on both the first and second invariants, the most complete mathematical description (linear, quadratic, cubic and exponential) stands out with the lowest error, showing approximately 0.52% error for HMPE and 1.77% error for PET. Additionally, the regressive criterion of the average error with the inclusion of the mathematical terms explored in this work is highlighted.

After presenting all graphical simulation results and mean error evaluations, it is worth emphasizing the exceptional performance of the proposed methodology, which enables constitutive numerical simulation of mechanical hysteresis directly calibrated with experimental data, with low computational cost and minimal errors, particularly for the complete mathematical formulation, Eq. (30). From a methodological perspective (rooted in continuum me-

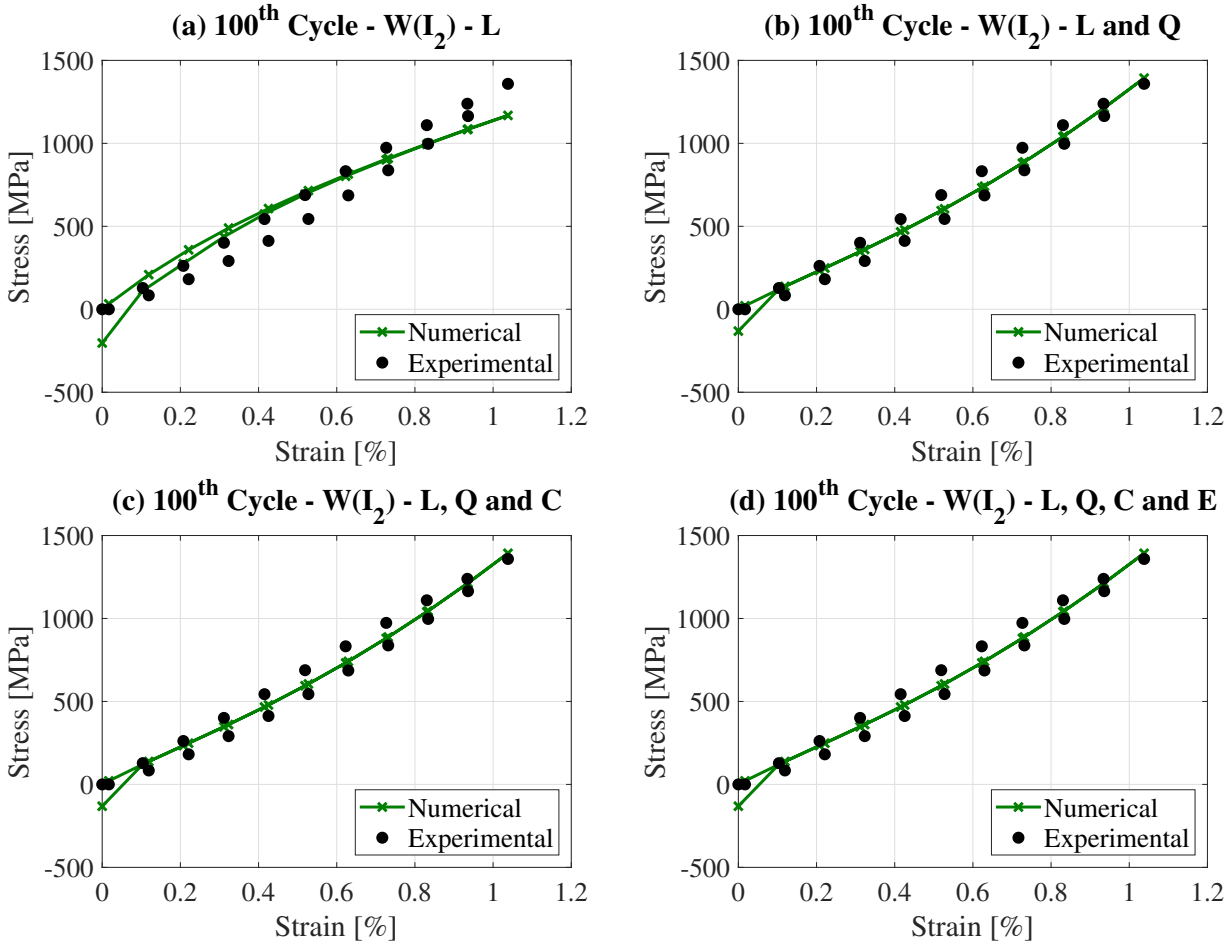

Figure 6: Numerical simulation for dependence on the second invariant, HMPE: (a) Linear; (b) Linear and quadratic; (c) Linear, quadratic and cubic; (d) Linear, quadratic, cubic and exponential.

Table 3: Average error in percentage for each numerical simulation, PET.

	$W(I_1)$	$W(I_2)$	$W(I_1, I_2)$
Linear	3.006	34.231	3.006
Linear and quadratic	2.606	19.657	2.606
Linear, quadratic and cubic	2.606	19.657	2.597
Linear, quadratic, cubic and exponential	2.606	19.657	1.766

chanics, stress and strain tensor formulations, and the adoption of a phenomenological hyperelastic strain energy function) such performance was expected, as this framework is well established in previous studies from the research group [30, 31, 32, 33, 34, 35, 36, 49].

Other studies in the literature have also addressed mechanical hysteresis simulation in different materials and contexts. Wen *et al.* [50] investigated the nonlinear mechanical behavior of flax-fiber-reinforced composites under loading–unloading cycles, developing a viscoelastic–plastic constitutive model. Although the study presented relevant findings, even with a detailed mathematical formulation and thorough parameter and geometry definitions, discrepancies between numerical and experimental stress–strain responses during dynamic cycles persisted. Gao *et al.* [51] focused on dynamic hysteresis compensation in tendon–sheath mechanisms for surgical robots, achieving excellent agreement between experimental measurements and elongation predictions. Shi *et al.* [52] examined the nonlinear hysteresis behavior of interlocked pseudo-metallic rubber under quasi-static compression, demonstrat-

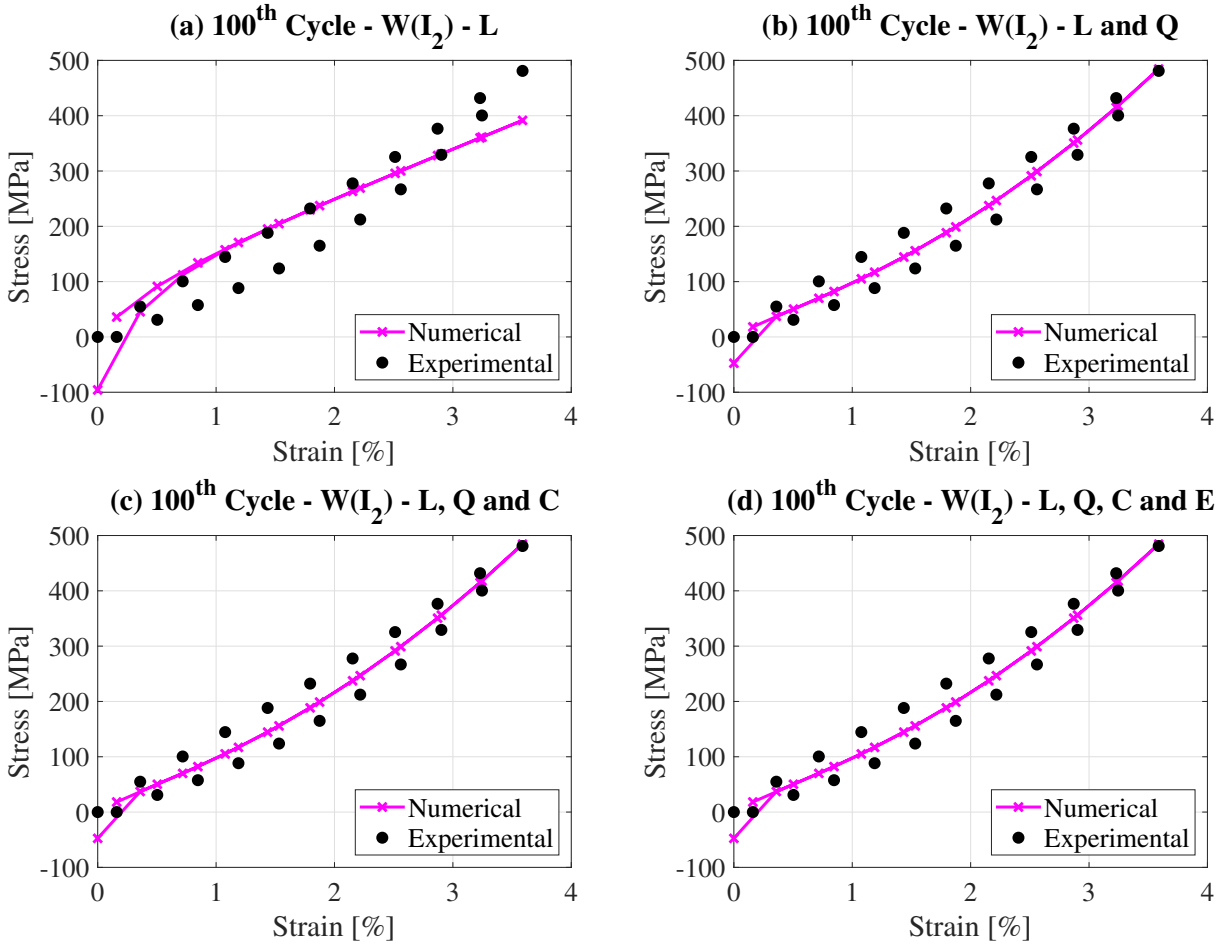

Figure 7: Numerical simulation for dependence on the second invariant, PET: (a) Linear; (b) Linear and quadratic; (c) Linear, quadratic and cubic; (d) Linear, quadratic, cubic and exponential.

ing that its hysteresis response can be decomposed into three mechanically significant components, with numerical predictions showing strong agreement with experimental validations.

These studies (cited in the previous paragraph) adopt highly robust methodologies, frequently relying on finite element methods or neural networks to replicate complex loading conditions. While the resulting numerical responses are often well validated, significant deviations from experimental data may still occur in such complex frameworks. In contrast, the methodology proposed herein offers a low-cost alternative focused on constitutive numerical simulation formulated as a parametric optimization problem. Despite not requiring geometric definition, mesh generation, or neural networks, the theoretical framework is consistent and rigorous, delivering excellent numerical predictions of stress–strain behavior, calibrated and validated against experimental data. And although some simplifications were applied in the present study (all duly justified), such as the assumptions of incompressibility, isotropy, and viscoelasticity for the fibers analyzed, the proposed framework remains capable of representing other materials and different characteristics, provided the corresponding developments are incorporated into the formulation.

It should be noted that, in the numerical simulation graphs of the hundredth cycle (Fig. 4, Fig. 5, Fig. 6, Fig. 7, Fig. 8 and Fig. 9), the peak strain is approximately 1.05% for HMPE and 3.6% for PET, while the experimental indications (Fig. 3) show a maximum strain of about 1.8% for HMPE and 8.0% for PET. This difference exists because the tensorial mathematical code starts from the known (undeformed) configuration to simulate numerically and perform the constants parametric optimization. In the simulations, the undeformed condition is the beginning of the hundredth cycle, which for simplicity in the numerical script is associated with the zero initial strain. Therefore, the peak strain shown in the numerical simulation graphs is related to the strain variation in the last cycle. Simulating for the actual strain values would lead to exactly the same numerical simulation curve and the same optimized result for the constants, with an additional term shifting the curve relative to the known (undeformed) condition.

Still focusing on the strain values, when analyzing the hundredth fatigue cycle, a proportion can be established relative to the rupture strain. As seen in the numerical simulation graphs, the strain variation of HMPE in the last cycle is 1.05%, which corresponds to approximately one-third of the HMPE rupture strain (0.35), while polyester

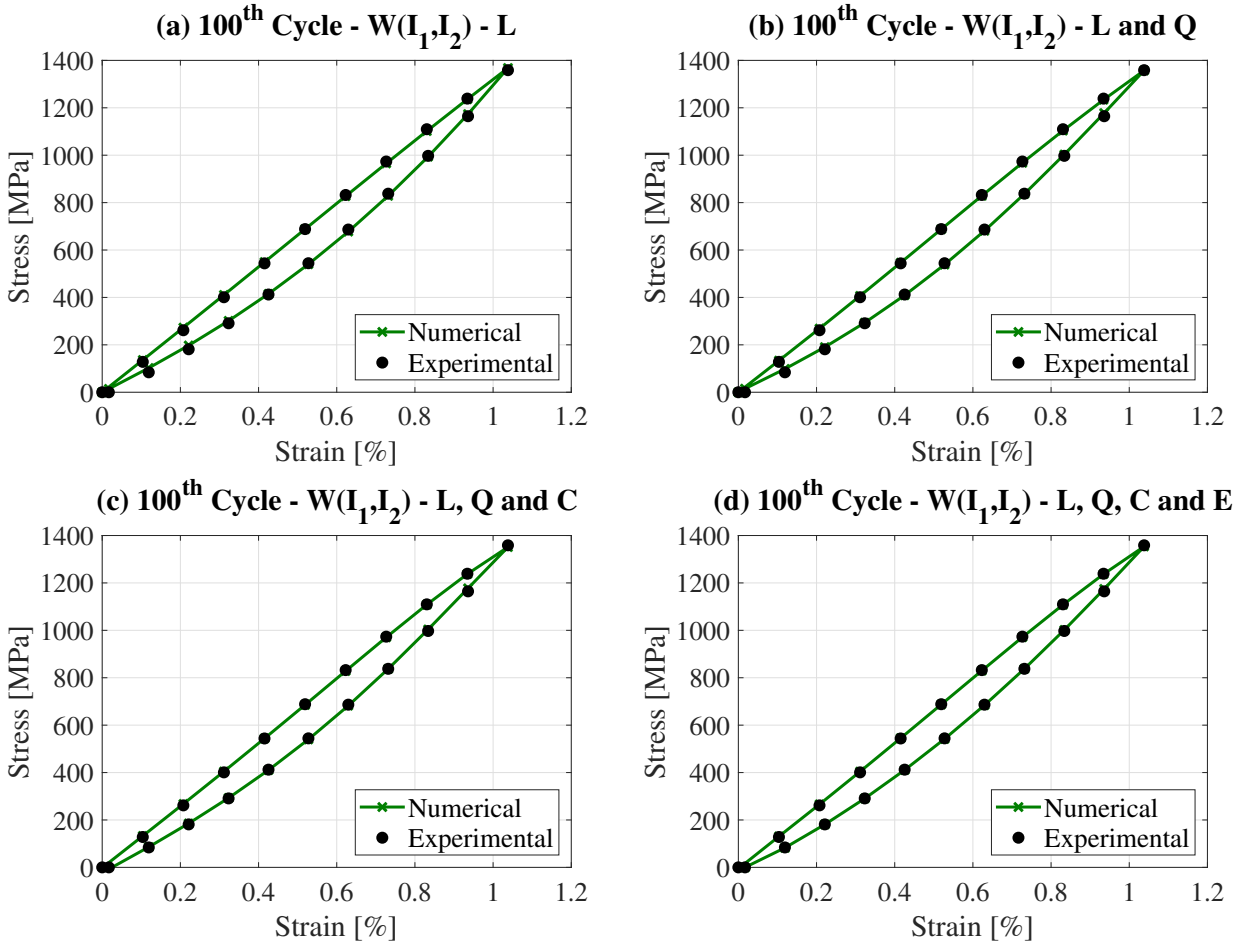

Figure 8: Numerical simulation for dependence on the first and second invariant, HMPE: (a) Linear; (b) Linear and quadratic; (c) Linear, quadratic and cubic; (d) Linear, quadratic, cubic and exponential.

shows a strain variation of 3.6% in the hundredth cycle, corresponding to about one-quarter of the PET rupture strain (0.27). Although this evaluation is not the primary focus here, based on the literature [24, 53], the normalized stiffness (K) can be calculated through Eq. (31), and it can be concluded that HMPE exhibits a greater gain in (K) compared to PET in the hundredth cycle, as indicated in Eq. (32), even though the strain gap is a larger fraction of the break strain.

$$K = \frac{(F_2 - F_1)/YBL}{(L_2 - L_1)/L_0} \tag{31}$$

$$K_{HMPE} = \frac{0.45}{0.0105} \approx 42.86 \neq K_{PET} = \frac{0.45}{0.036} \approx 12.50 \tag{32}$$

Although it is not the main focus of the present work, it is possible to compare the normalized stiffness values obtained with those reported in the literature. Lian *et al.* [54] investigated the effect of bedding-in on the mechanical behavior of aramid, HMPE, and polyester ropes, performing several evaluations of normalized stiffness under dynamic cycles. One of the graphs presented for the 100th cycle shows a well-defined mechanical hysteresis loop, and for the loading condition between 16% and 64% of the Minimum Break Strength (MBS), representing Δ48%MBS, the dynamic stiffness in the 100th cycle (without bedding-in) was reported as 70.03 for HMPE and 23.68 for polyester. These values reported by Lian *et al.* [54] refer to ropes with specific constructive characteristics and, when compared with the values presented in Eq. (32), are naturally different because they correspond to another constructive level (multifilaments). Nevertheless, the proportionality is maintained, with the stiffness of HMPE being approximately three times higher than that of PET.

All simulations represented in Fig. 4 and Fig. 5 for $W(I_1)$, in Fig. 6 and Fig. 7 for $W(I_2)$, in Fig. 8 and Fig. 9 for $W(I_1, I_2)$ pertain to a set of optimized constants that numerically simulate the constitutive behavior. Naturally, the more constants a given strain energy function has, the higher the computational cost and processing time. Table 4 displays all the constant values obtained in each simulation for HMPE, and Table 5 for PET.

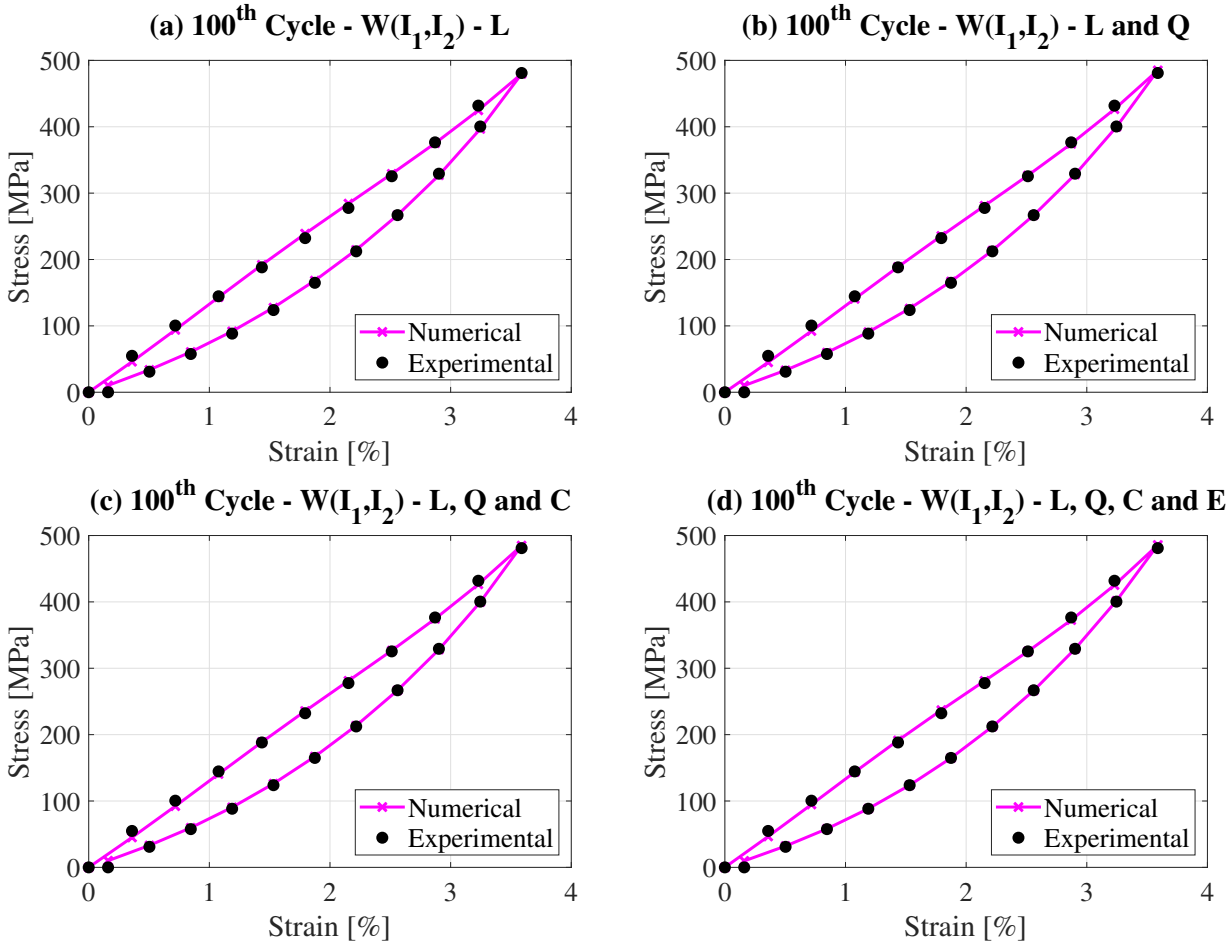

Figure 9: Numerical simulation for dependence on the first and second invariant, PET: (a) Linear; (b) Linear and quadratic; (c) Linear, quadratic and cubic; (d) Linear, quadratic, cubic and exponential.

Table 4: Optimized constants for each numerical simulation, HMPE.

	$W(I_1)$				$W(I_2)$				$W(I_1, I_2)$			
	L	LQ	LQC	LQCE	L	LQ	LQC	LQCE	L	LQ	LQC	LQCE
γ	0.50	0.50	0.50	0.50	0.50	0.50	0.50	0.50	0.50	0.50	0.50	0.50
τ	160.29	160.07	160.07	160.07	0.67	0.03	0.03	0.03	160.29	132.93	294.06	660.89
C_1	218.43	218.31	218.31	211.59	650.52	420.76	420.76	411.35	218.43	214.23	210.80	0.40
C_2	–	0.10	0.10	0.10	–	134.54	134.54	134.54	3×10^{-8}	3×10^{-7}	5.90	4.45
C_3	–	–	8×10^{-8}	5×10^{-8}	–	–	2.1×10^{-6}	4.4×10^{-7}	–	12.66	1.2×10^{-5}	1.1×10^{-3}
C_4	–	–	–	6.72	–	–	–	9.41	–	12.62	18.80	15.41
C_5	–	–	–	1.5×10^{-4}	–	–	–	3.7×10^{-4}	–	–	10.10	5.80
C_6	–	–	–	–	–	–	–	–	–	–	18.30	8.34
C_7	–	–	–	–	–	–	–	–	–	–	–	405.37
C_8	–	–	–	–	–	–	–	–	–	–	–	882.63
C_9	–	–	–	–	–	–	–	–	–	–	–	13.52
C_{10}	–	–	–	–	–	–	–	–	–	–	–	21.19

Table 5: Optimized constants for each numerical simulation, PET.

	$W(I_1)$				$W(I_2)$				$W(I_1, I_2)$			
	L	LQ	LQC	LQCE	L	LQ	LQC	LQCE	L	LQ	LQC	LQCE
γ	0.50	0.50	0.50	0.50	0.50	0.50	0.50	0.50	0.50	0.50	0.50	0.50
τ	22.68	22.45	22.45	22.45	0.25	0.02	0.03	0.02	22.68	22.45	22.50	21.00
C_1	21.15	20.76	20.76	7.45	86.22	42.79	42.79	24.24	21.15	20.76	20.75	20.08
C_2	–	0.02	0.02	0.02	–	5.13	5.13	5.13	3×10^{-8}	1×10^{-8}	1×10^{-8}	9×10^{-8}
C_3	–	–	3×10^{-8}	3×10^{-8}	–	–	1.4×10^{-7}	0.00	–	0.02	0.02	0.05
C_4	–	–	–	13.31	–	–	–	18.56	–	2×10^{-8}	0.00	1×10^{-8}
C_5	–	–	–	5.6×10^{-5}	–	–	–	2.8×10^{-5}	–	–	0.00	0.00
C_6	–	–	–	–	–	–	–	–	–	–	3.3×10^{-5}	5.7×10^{-4}
C_7	–	–	–	–	–	–	–	–	–	–	–	2.77
C_8	–	–	–	–	–	–	–	–	–	–	–	898.17
C_9	–	–	–	–	–	–	–	–	–	–	–	8.5×10^{-7}
C_{10}	–	–	–	–	–	–	–	–	–	–	–	59.78

As can be observed in the constant values, some coefficients are very close to zero and therefore virtually cancel out the associated mathematical terms. This indicates the mathematical significance of the model concerning the terms accompanying each coefficient.

In the constants presented, both in Table 4 and Table 5, the values for gamma (γ) stand out, representing a portion of stiffness related to the descriptive tensorial viscoelastic model used to determine the final Piola-Kirchhoff stress tensor $\boldsymbol{S}_{final}$, as indicated in Eq. (15). This is because this value remains constant at 0.5 for all simulations and for different fibers, which might be understandable as a general property of polymeric fibers related to the developed model. Regarding the other constant values listed in Table 4 and Table 5, although there is some similarity in certain cases, it is very difficult and premature to make any definitive statement about the behavior of the constants in relation to each numerical simulation.

It is worth emphasizing that, in the context of reducing computational cost, all models employed in the present work are phenomenological and do not carry explicit physical or mechanical meaning for their constants. This is precisely what makes it challenging to interpret and correlate the values of the constants obtained and shown in Table 4 and Table 5. Several studies in the literature have employed these models. For instance, Zhang *et al.* [55] addressed the numerical simulation of thermomechanical coupling in rubbers using the Yeoh model, which differs slightly from the model used in the present work, Eq. (21), as it includes terms dependent on temperature and the Jacobian (volume change), which is the focus of their analysis. Other studies have also developed phenomenological hyperelastic strain energy functions for isotropic materials based on Ogden-type polynomials, exponential components, and Baker–Ericksen inequalities, among others [56, 57, 58]. The dissertation by Hoss [59] provides a comprehensive overview of different hyperelastic constitutive models, presenting both phenomenological and micromechanical formulations.

The application of micromechanical models, although theoretically more rigorous, poses significant practical challenges. These models require an extensive and accurate set of physical and mechanical information, often demanding a complete and detailed material characterization at multiple scales [60]. In addition, they generally involve higher computational costs and, in many cases, exhibit numerical convergence issues, particularly when applied to complex geometries or nonlinear loading conditions, and are thus more commonly used for heterogeneous problems [61]. For these reasons, in polymers, rubbers, and synthetic fibers, phenomenological models are more commonly adopted. Frequently coupled with hyperelastic and/or viscoelastic formulations, these models, although less descriptive at the microscopic level (material physical and mechanical information), offer greater robustness and feasibility for numerical simulations with experimental calibration.

In the methodology used, the experimental execution of a dynamic load cycling test stands out, but the numerical simulation performed is only for the hundredth and final load-unload cycle. Considering the characteristics of these fibers, they are viscoelastic materials that typically exhibit behaviors such as creep, stress relaxation, or mechanical hysteresis, and the mathematical-numerical development itself takes into account their viscoelastic nature. In fact, during mechanical tests under cyclic loading, there is a stabilization of mechanical hysteresis, a phenomenon also reported in some works in the literature [6, 11, 12, 62]. As these inelastic portions of the material are gradually eliminated cycle by cycle, the stress-strain behavior becomes more homogeneous.

In the present work, when performing the numerical simulation for the most stabilized cycle (100th cycle), an excellent convergence between numerical and experimental results is achieved (provided there is dependence on

the first invariant of continuum mechanics, I_1). In fact, the numerical simulation routine calibrated through experimental tests proves to be very efficient in cycle-by-cycle simulation, where each cycle is simulated individually. Not surprisingly, the mathematical descriptions of the strain energy model are based on a phenomenological approach, as they capture the phenomenon and, when compared with experimental data, generate a numerical curve that fits very well. However, the model is incapable of numerically simulating all 100 dynamic cycles experimentally conducted using the same set of constants. If the constants obtained in the hundredth cycle were applied to the first cycle, the shape of the curve would be identical but significantly shifted in relation to the strain.

When considering a stiffness criterion, one could infer that the application of loadings, such as quasi-static loads, before performing the dynamic cycling could reduce this effect, allowing the constants to be valid for all cycles, thereby simulating the stress-strain behavior for the entire cyclic loading and not just for the last cycle. However, this inference is refuted in the work by da Cruz *et al.* [36], which shows a similar scenario where successive dynamic cycles are numerically simulated after quasi-static stages. Even so, the numerical model is extremely effective for cycle-by-cycle simulation but inefficient at providing a single set of constants that can simulate all successive dynamic cycles. Therefore, it is not only to consider the elimination of inelastic portions but also to address damage, and more, the accumulation of damage throughout the cycles. Perhaps the set of constants and their changes over the cycles reflect an interaction between two factors: the removal of inelastic portions and the accumulation of damage.

4 Conclusions

In conclusion, it can be understood that the dependence on the first strain invariant (I_1) is necessary for the numerical description of the constitutive behavior of synthetic polymer fibers. This invariant is related to the sum of principal strains that exist mainly longitudinally in the fibers. The mathematical model with the lowest average error encompasses a complete mathematical description of the terms studied in this work and depends on the invariants I_1 and I_2. Thus, it is also understandable that the use of the second invariant complements the numerical-mathematical description, optimizing the simulation.

The purely linear model dependent on I_1, known in the literature as the Neo-Hookean model, shows good convergence of results with a reduced number of constants for simulation, confirming that for these synthetic materials, the most significant terms are the linear ones of the principal stretches. And also representing a simplifying possibility by using a model with a low number of constants, reducing the computational cost while still presenting small average errors.

The Modified Yeoh model was used as the basis for this work because it presented in literature the lowest error in the simulation for polyester fibers. This model understands the primary dependence of the simulation on the first invariant (I_1), additionally, the variety of mathematical descriptions offered by the Modified Yeoh model explains its better performance compared to other nominal models (Bechir-Boufala-Chevalier, Hartmann-Neff, Mooney-Rivlin, Neo-Hook, Stumpf-Marczak and Yeoh). Further mathematical exploration in future studies could be conducted by incorporating other types of mathematical terms into the equation, such as inverse and logarithmic terms.

Additionally, for future studies, more detailed exploration of the relationships between mathematical terms and strain invariants can be pursued. Perhaps the most optimized model would be a mathematical construction where some terms depend on I_1 and others on I_2, without both invariants being present in the mathematical formulation of mechanical behavior. Thus, rather than being merely additive and progressive (as in this work), future models could consist of mathematical terms with meaningful coefficients and your sensitivity for simulation, regardless of the type of dependence on the strain invariants or the specific mathematical terms.

In summary, the initial gaps outlined in this study—namely, (i) the need to simulate stabilized hysteresis behavior in synthetic fibers, (ii) to evaluate different mathematical terms in the strain energy function, and (iii) to investigate the influence of invariants I_1 and I_2—were directly addressed throughout the analysis. Most notably, the proposed numerical methodology proved to be suitable, achieving low simulation errors under various conditions while maintaining reduced computational cost. The results confirmed the predominance of I_1 in capturing the mechanical behavior, whereas the inclusion of I_2 improved numerical performance; however, I_2-dependent terms alone were insufficient to fully represent the constitutive behavior of the fibers. Furthermore, the analysis of different mathematical formulations showed that linear terms remain dominant, although combinations with higher-order and exponential terms can improve accuracy. These findings support the development of more efficient and computationally optimized constitutive models for offshore polymeric fibers and establish a solid foundation for future studies on model refinement and simplification.

Acknowledgements

This study was financed in part by the Coordenação de Aperfeiçoamento de Pessoal de Nível Superior – Brasil (CAPES) – Finance Code 001, besides Conselho Nacional de Desenvolvimento Científico e Tecnológico – CNPq

(Grant n° 307889/2022). Thanks also to the funding agencies: Finep, FAPERGS, and FAPERJ.

References

[1] E. Hage Jr, "Aspectos históricos sobre o desenvolvimento da ciência e da tecnologia de polímeros," *Polímeros*, vol. 8, no. 2, pp. 6–9, 1998. Available at: https://doi.org/10.1590/S0104-14281998000200003

[2] W. D. Callister Jr, *Ciência e engenharia de materiais: uma introdução*, 7ª ed. Rio de Janeiro, Brasil: Editora LTC, 2008.

[3] C. J. M. Del Vecchio, "Light weight materials for deep water moorings," Doctoral thesis, University of Reading, Reading, UK, 1992. Available at: https://go.exlibris.link/4jFtzQrc

[4] L. F. Haach, D. T. Poitevin, and M. B. Bastos, "Prospects of synthetic fibers for deepwater mooring," in *Rio Oil & Gas Expo and Conference*. Rio de Janeiro, Brazil: IBP, 2010.

[5] H. A. McKenna, J. W. S. Hearle, and N. O'Hear, *Handbook of fibre rope technology*. Sawston, Cambridge, UK: Woodhead Publishing, 2004, vol. 34.

[6] H. Liu, W. Huang, Y. Lian, and L. Li, "An experimental investigation on nonlinear behaviors of synthetic fiber ropes for deepwater moorings under cyclic loading," *Applied Ocean Research*, vol. 45, pp. 22–32, 2014. Available at: https://doi.org/10.1016/j.apor.2013.12.003

[7] C. Barrera, R. Guanche, and I. J. Losada, "Experimental modelling of mooring systems for floating marine energy concepts," *Marine Structures*, vol. 63, pp. 153–180, 2019. Available at: https://doi.org/10.1016/j.marstruc.2018.08.003

[8] D. M. da Cruz, A. Penaquioni, L. B. Zangalli, M. B. Bastos, I. N. Bastos, and A. L. N. da Silva, "Non-destructive testing of high-tenacity polyester sub-ropes for mooring systems," *Applied Ocean Research*, vol. 134, p. 103513, 2023. Available at: https://doi.org/10.1016/j.apor.2023.103513

[9] S. D. Weller, L. Johanning, P. Davies, and S. J. Banfield, "Synthetic mooring ropes for marine renewable energy applications," *Renewable Energy*, vol. 83, pp. 1268–1278, 2015. Available at: https://doi.org/10.1016/j.renene.2015.03.058

[10] M. B. Bastos, E. B. Fernandes, and A. L. N. da Silva, "Performance fibers for deep water offshore mooring ropes: Evaluation and analysis," in *OCEANS 2016 - Shanghai*. Shanghai, China: IEEE, 2016, pp. 169–177. Available at: https://doi.org/10.1109/OCEANSAP.2016.7485612

[11] P. Davies, Y. Reaud, L. Dussud, and P. Woerther, "Mechanical behaviour of HMPE and aramid fibre ropes for deep sea handling operations," *Ocean Engineering*, vol. 38, no. 17–18, pp. 2208–2214, 2011. Available at: https://doi.org/10.1016/j.oceaneng.2011.10.010

[12] D. M. da Cruz, M. A. Barreto, L. B. Zangalli, A. J. da Cruz Júnior, I. Melito, F. M. Clain, and C. E. M. Guilherme, "Mechanical characterization procedure of HMPE fiber for offshore mooring in deep waters," *Engineering Solid Mechanics*, vol. 12, no. 3, pp. 311–322, 2024. Available at: https://doi.org/10.5267/j.esm.2024.1.003

[13] M. P. Vlasblom and R. L. Bosman, "Predicting the creep lifetime of HMPE mooring rope applications," in *OCEANS 2006*. Boston, MA, USA: IEEE, 2006, pp. 1–10. Available at: https://doi.org/10.1109/OCEANS.2006.307013

[14] M. Vlasblom, J. Boesten, S. Leite, and P. Davies, "Development of HMPE fiber for permanent deepwater offshore mooring," in *Offshore Technology Conference*, Houston, Texas, USA, 2012, pp. OTC–23 333–MS. Available at: https://doi.org/10.4043/23333-MS

[15] R. Bosman, Q. Zhang, A. Leao, and C. Godreau, "First class certification on HMPE fiber ropes for permanent floating wind turbine mooring system," in *Offshore Technology Conference*, Houston, Texas, USA, 2020, pp. OTC–30 475–MS. Available at: https://doi.org/10.4043/30475-MS

[16] D. M. da Cruz, M. A. Barreto, L. B. Zangalli, T. L. Popiolek Júnior, and C. E. M. Guilherme, "Experimental study of creep behavior at high temperature in different HMPE fibers used for offshore mooring," in *Offshore Technology Conference Brasil*, Rio de Janeiro, Brazil, 2023, pp. OTC–32 760–MS. Available at: https://doi.org/10.4043/32760-MS

[17] E. L. V. Louzada, C. E. M. Guilherme, and F. T. Stumpf, "Evaluation of the fatigue response of polyester yarns after the application of abrupt tension loads," *Acta Polytechnica CTU Proceedings*, vol. 7, pp. 76–78, 2016. Available at: https://doi.org/10.14311/APP.2017.7.0076

[18] S. R. Ghoreishi, P. Davies, P. Cartraud, and T. Messager, "Analytical modeling of synthetic fiber ropes. part ii: A linear elastic model for 1 + 6 fibrous structures," *International Journal of Solids and Structures*, vol. 44, no. 9, pp. 2943–2960, 2007. Available at: https://doi.org/10.1016/j.ijsolstr.2006.08.032

[19] W. Huang, H. Liu, Y. Lian, and L. Li, "Modeling nonlinear creep and recovery behaviors of synthetic fiber ropes for deepwater moorings," *Applied Ocean Research*, vol. 39, pp. 113–120, 2013. Available at: https://doi.org/10.1016/j.apor.2012.10.004

[20] V. Sry, Y. Mizutani, G. Endo, Y. Suzuki, and A. Todoroki, "Consecutive impact loading and preloading effect on stiffness of woven synthetic-fiber rope," *Journal of Textile Science and Technology*, vol. 3, no. 1, pp. 1–16, 2017. Available at: https://doi.org/10.4236/jtst.2017.31001

[21] S. Xu, S. Wang, and C. G. Soares, "Experimental investigation on hybrid mooring systems for wave energy converters," *Renewable Energy*, vol. 158, pp. 130–153, 2020. Available at: https://doi.org/10.1016/j.renene.2020.05.070

[22] E. S. Belloni, F. M. Clain, and C. E. M. Guilherme, "Post-impact mechanical characterization of HMPE yarns," *Acta Polytechnica*, vol. 61, no. 3, pp. 406–414, 2021. Available at: https://doi.org/10.14311/AP.2021.61.0406

[23] D. M. da Cruz, F. M. Clain, and C. E. M. Guilherme, "Experimental study of the torsional effect for yarn break load test of polymeric multifilaments," *Acta Polytechnica*, vol. 62, no. 5, pp. 538–548, 2022. Available at: https://doi.org/10.14311/AP.2022.62.0538

[24] I. Melito, D. M. da Cruz, E. S. Belloni, F. M. Clain, and C. E. M. Guilherme, "The effects of mechanical degradation on the quasi static and dynamic stiffness of polyester yarns," *Engineering Solid Mechanics*, vol. 11, no. 3, pp. 243–252, 2023. Available at: https://doi.org/10.5267/j.esm.2023.4.001

[25] H. H. Pham, "Numerical modeling of a mooring line system for an offshore floating wind turbine in vietnamese sea conditions using nonlinear materials," *Water Science and Engineering*, vol. 17, no. 3, pp. 300–308, 2024. Available at: https://doi.org/10.1016/j.wse.2023.10.004

[26] I. Tsukrov, O. Eroshkin, W. Paul, and B. Celikkol, "Numerical modeling of nonlinear elastic components of mooring systems," *IEEE Journal of Oceanic Engineering*, vol. 30, no. 1, pp. 37–46, 2005. Available at: https://doi.org/10.1109/JOE.2004.841396

[27] C. Cifuentes, S. Kim, M. H. Kim, and W. S. Park, "Numerical simulation of the coupled dynamic response of a submerged floating tunnel with mooring lines in regular waves," *Ocean Systems Engineering*, vol. 5, no. 2, pp. 109–123, 2015. Available at: https://doi.org/10.12989/ose.2015.5.2.109

[28] N. Nguyen and K. Thiagarajan, "Nonlinear viscoelastic modeling of synthetic mooring lines," *Marine Structures*, vol. 85, p. 103257, 2022. Available at: https://doi.org/10.1016/j.marstruc.2022.103257

[29] M. Chen, C. B. Li, Z. Han, and J. bin Lee, "A simulation technique for monitoring the real-time stress responses of various mooring configurations for offshore floating wind turbines," *Ocean Engineering*, vol. 278, p. 114366, 2023. Available at: https://doi.org/10.1016/j.oceaneng.2023.114366

[30] F. T. Stumpf, C. E. M. Guilherme, D. M. da Cruz, A. H. M. F. T. da Silva, and M. B. Bastos, "A general constitutive model for the numerical simulation of different synthetic fibres used in offshore mooring," *Ships and Offshore Structures*, vol. 18, no. 9, pp. 1338–1344, 2023. Available at: https://doi.org/10.1080/17445302.2022.2116766

[31] D. M. da Cruz, C. E. M. Guilherme, F. T. Stumpf, and M. B. Bastos, "Numerical assessment of mechanical behavior of mooring lines using hybrid synthetic fiber-rope segments," in *Offshore Technology Conference*, Houston, Texas, USA, 2022, pp. OTC–31 906–MS. Available at: https://doi.org/10.4043/31906-MS

[32] F. T. Stumpf, M. A. Barreto, D. M. da Cruz, and C. E. M. Guilherme, "Numerical simulation of multi-material hybrid lines for offshore mooring," *Ocean Engineering*, vol. 305, p. 117979, 2024. Available at: https://doi.org/10.1016/j.oceaneng.2024.117979

[33] D. M. da Cruz, T. L. Popiolek Júnior, M. A. Barreto, C. E. M. Guilherme, and F. T. Stumpf, "Evaluation of energy models for numerical simulation of the mechanical behavior of polyester multifilaments," *The Journal of Engineering and Exact Sciences*, vol. 9, no. 1, p. 15321–01e, 2023. Available at: https://doi.org/10.18540/jcecvl9iss1pp15321-01e

[34] D. M. da Cruz, M. A. Barreto, L. B. Zangalli, F. T. Stumpf, J. M. Vassoler, and C. E. M. Guilherme, "Numerical simulation of the stress-strain behavior of polymeric fibers for mooring offshore structures," in *XLIV Ibero-Latin American Congress on Computational Methods in Engineering*. Porto, Portugal: ABMEC, 2023. Available at: https://publicacoes.softaliza.com.br/cilamce2023/article/view/4900

[35] D. M. da Cruz, T. L. Popiolek Júnior, M. A. Barreto, S. P. de Souza, L. B. Zangalli, A. J. da Cruz Júnior, T. C. Martins, A. L. N. da Silva, I. N. Bastos, and C. E. M. Guilherme, "Numerical simulation with hyperelastic constitutive model for high-performance multifilaments used in offshore mooring ropes," *The Journal of Engineering and Exact Sciences*, vol. 10, no. 2, p. 17255, 2024. Available at: https://doi.org/10.18540/jcecvl10iss2pp17255

[36] D. M. da Cruz, L. B. Zangalli, M. A. Barreto, I. N. Bastos, and A. L. N. da Silva, "Numerical simulation of the stress-strain behavior of polyester subropes for offshore mooring and relationship with change stiffness during the test protocol," in *ROG.e*. Rio de Janeiro, Brazil: IBP, 2024. Available at: https://doi.org/10.48072/2525-7579.roge.2024.3215

[37] American Society for Testing and Materials, *D1577 Standard Test Methods for Linear Density of Textile Fibers*, ASTM, West Conshohocken, Pennsylvania, USA, 2018. Available at: https://doi.org/10.1520/D1577-07R18

[38] International Organization for Standardization, *2062 Textiles — Yarns from packages — Determination of single-end breaking force and elongation at break using constant rate of extension (CRE) tester*, ISO, Geneva, Switzerland, 2009. Available at: https://www.iso.org/standard/45642.html

[39] J. C. Simo and T. J. R. Hughes, *Computational Inelasticity*. New York, USA: Springer-Verlag, 1997.

[40] P. J. Flory, "Thermodynamic relations for high elastic materials," *Transactions of the Faraday Society*, vol. 57, pp. 829–838, 1961. Available at: https://doi.org/10.1039/TF9615700829

[41] G. A. Holzapfel, *Nonlinear Solid Mechanics: A Continuum Approach for Engineering Science*. Chichester, UK: John Wiley & Sons, 2000.

[42] O. H. Yeoh, "Some forms of the strain energy function for rubber," *Rubber Chemistry and Technology*, vol. 66, no. 5, pp. 754–771, 1993. Available at: https://doi.org/10.5254/1.3538343

[43] R. S. Rivlin, "Large elastic deformations of isotropic materials iv. further developments of the general theory," *Philosophical Transactions of the Royal Society of London. Series A, Mathematical and Physical Sciences*, vol. 241, no. 835, pp. 379–397, 1948. Available at: https://doi.org/10.1098/rsta.1948.0024

[44] O. H. Yeoh, "Characterization of elastic properties of carbon-black-filled rubber vulcanizates," *Rubber Chemistry and Technology*, vol. 63, no. 5, pp. 792–805, 1990. Available at: https://doi.org/10.5254/1.3538343

[45] M. Mooney, "A theory of large elastic deformation," *Journal of Applied Physics*, vol. 11, no. 9, pp. 582–592, 1940. Available at: https://doi.org/10.1063/1.1712836

[46] R. S. Rivlin and D. W. Saunders, "Large elastic deformations of isotropic materials vii. experiments on the deformation of rubber," *Philosophical Transactions of the Royal Society of London. Series A, Mathematical and Physical Sciences*, vol. 243, no. 865, pp. 251–288, 1951. Available at: https://doi.org/10.1098/rsta.1951.0004

[47] International Organization for Standardization, *18692-3 Fibre ropes for offshore stationkeeping — Part 3: High modulus polyethylene (HMPE)*, ISO, Geneva, Switzerland, 2020. Available at: https://www.iso.org/standard/77487.html

[48] ——, *18692-2 Fibre ropes for offshore stationkeeping — Part 2: Polyester*, ISO, Geneva, Switzerland, 2019. Available at: https://www.iso.org/standard/70290.html

[49] D. M. da Cruz, L. B. Zangalli, M. A. Barreto, A. L. N. da Silva, and I. N. Bastos, "Numerical simulation of creep behavior in low creep HMPE fibers used for offshore mooring ropes," in *Offshore Technology Conference Brasil*, Rio de Janeiro, Brazil, 2025, pp. OTC–36 033–MS. Available at: https://doi.org/10.4043/36033-MS

[50] B. Wen, J. Zhang, Q. Li, Z. Zhang, and H. Ding, "A novel visco-elastic–plastic constitutive model for predicting the cyclic loading–unloading nonlinear tensile behaviors of off-axis twisted flax fiber reinforced composites," *Composites Part A: Applied Science and Manufacturing*, vol. 190, no. 6, p. 108679, 2025. Available at: https://doi.org/10.1016/j.compositesa.2024.108679

[51] Q. Gao, G. Ji, M. Sun, Y. Xiao, H. Rao, and Z. Sun, "Dynamic hysteresis compensation for tendon-sheath mechanism in flexible surgical robots without distal perception," *IEEE Transactions on Robotics*, vol. 41, pp. 3703–3721, 2025. Available at: https://doi.org/10.1109/TRO.2025.3577011

[52] L. Shi, Q. Wang, L. Shen, L. Pang, J. Huang, and Z. Ren, "Influence of self-contact friction on the hysteresis mechanical behavior of entangled metal pseudo rubber," *Tribology International*, vol. 209, p. 110765, 2025. Available at: https://doi.org/10.1016/j.triboint.2025.110765

[53] F. Khalid, P. Davies, P. Halswell, N. Lacotte, P. R. Thies, and L. Johanning, "Evaluating mooring line test procedures through the application of a round robin test approach," *Journal of Marine Science and Engineering*, vol. 8, no. 6, p. 436, 2020. Available at: https://doi.org/10.3390/jmse8060436

[54] Y. Lian, Y. Zhang, Y. Xie, J. Zheng, W. Chen, S.-C. Chen, J. Zhang, M.-A. Xue, and S. C. Yim, "Effects of bedding-in loading history on mechanical behaviors of aramid HMPE and polyester mooring ropes," *Ocean Engineering*, vol. 321, p. 120413, 2025. Available at: https://doi.org/10.1016/j.oceaneng.2025.120413

[55] L. Zhang, Z. Li, Q. Fu, N. Tang, S. Pan, M. Lin, B. Wang, P. Bai, D. Qiao, B. Zhang, and F. Huang, "High-precision numerical simulation method for thermal–mechanical coupling in rubbers," *Polymer Engineering & Science*, vol. 65, no. 1, pp. 120–134, 2025. Available at: https://doi.org/10.1002/pen.26996

[56] M. Bahreman, H. Darijani, and M. Fooladi, "Constitutive modeling of isotropic hyperelastic materials using proposed phenomenological models in terms of strain invariants," *Polymer Engineering & Science*, vol. 56, no. 3, pp. 299–308, 2016. Available at: https://doi.org/10.1002/pen.24255

[57] F. T. Stumpf and R. J. Marczak, "Constitutive framework of a new hyperelastic model for isotropic rubber-like materials for finite element implementation," *Latin American Journal of Solids and Structures*, vol. 18, no. 2, p. e346, 2021. Available at: https://doi.org/10.1590/1679-78256349

[58] N. H. Shah and S. F. Ali, "A hyperelastic strain energy function for isotropic rubberlike materials," *International Journal of Mechanical Sciences*, vol. 279, p. 109472, 2024. Available at: https://doi.org/10.1016/j.ijmecsci.2024.109472

[59] L. Hoss, "Modelos constitutivos hiperelásticos para elastômeros incompressíveis: ajuste, comparação de desempenho e proposta de um novo modelo [in portuguese]," Master's thesis, Universidade Federal do Rio Grande do Sul, Porto Alegre, Brazil, 2009. Available at: http://hdl.handle.net/10183/16310

[60] M. Kachanov and I. Sevostianov, *Micromechanics of Materials, with Applications*, ser. Solid Mechanics and Its Applications. Cham, Switzerland: Springer, 2018. Available at: https://doi.org/10.1007/978-3-319-76204-3

[61] V. A. Buryachenko, *Local and Nonlocal Micromechanics of Heterogeneous Materials*. Cham, Switzerland: Springer, 2022. Available at: https://doi.org/10.1007/978-3-030-81784-8

[62] H. Thuilliez, P. Davies, P. Cartraud, M. Feuvrie, and T. Soulard, "Characterization and modelling of the dynamic stiffness of nylon mooring rope for floating wind turbines," *Ocean Engineering*, vol. 287, p. 115866, 2023. Available at: https://doi.org/10.1016/j.oceaneng.2023.115866